Journal of Alloys and Compounds 757 (2018) 403–414

Contents lists available at ScienceDirect

Journal of Alloys and Compounds

journal homepage: http://www.elsevier.com/locate/jalcom

Effect of Cr and Zr on phase stability of refractory Al-Cr-Nb-Ti-V-Zr high-entropy alloys

N.Yu. Yurchenko [a, *], N.D. Stepanov [a], A.O. Gridneva [a], M.V. Mishunin [b], G.A. Salishchev [a], S.V. Zherebtsov [a]

[a] Laboratory of Bulk Nanostructured Materials, Belgorod State National Research University, Belgorod, 308015, Russia
[b] Laboratory of Radiation Physics, Belgorod State National Research University, Belgorod, 308015, Russia

ARTICLE INFO

Article history:
Received 20 March 2018
Received in revised form
7 May 2018
Accepted 8 May 2018
Available online 10 May 2018

Keywords:
High entropy alloys
Microstructure
Phase transitions
Mechanical properties
Scanning electron microscopy
SEM
Transmission electron microscopy
TEM

ABSTRACT

The effect of annealing at 800 °C or 1000 °C for 100 h on the structure and mechanical properties of refractory $AlCr_xNbTiV$ and $AlNbTiVZr_x$ (x = 0–1.5) high-entropy alloys was studied. In the initial condition (annealing at 1200 °C for 24 h), the AlNbTiV and $AlCr_{0.5}NbTiV$ alloys were composed of the B2 phase while the AlCrNbTiV and $AlCr_{1.5}NbTiV$ alloys had a mixture of the B2 and Cr_2Nb-type C14 Laves phases. The $AlNbTiVZr_x$ (x = 0.5–1.5) alloys in the initial condition consisted of the B2, Zr_5Al_3-type, and ZrAlV-type C14 Laves phases. Annealing of the $AlCr_xNbTiV$ (x = 0–1.5) alloys at 800 °C or 1000 °C resulted in (i) precipitation of the Nb_2Al-type σ-phase or an increase in the fraction of the Laves phase; (ii) an increase in the microhardness and a pronounced drop in ductility. Annealings of the $AlNbTiVZr_x$ (x = 0.5–1.5) alloys at 800 °C or 1000 °C led to insignificant changes in the structure and microhardness but somewhat decreased ductility. Quasi-binary AlNbTiV-Cr and AlNbTiV-Zr phase diagrams constructed with a Thermo-Calc software and TCHEA2 database were used to analyze phase transformations in the experimental alloys. The differences in the behavior of the Cr/Zr-containing alloys and the relationships between the phase composition and mechanical properties of the alloys were discussed.

© 2018 Elsevier B.V. All rights reserved.

1. Introduction

High-entropy alloys (HEAs) are a relatively new class of metallic alloys intensively studied over the past two decades [1–5]. According to the original definition, HEAs are alloys consisting of at least 5 elements taken in equimolar concentrations [1]. Due to unique mechanical properties, which can exceed those of conventional alloys and/or fill gaps between characteristics of existing alloys, HEAs are considered as promising candidates for different potential applications [6].

One of the most perspective usages for HEAs is associated with the production of high-temperature structural materials. The first-developed HEAs based on refractory metals (refractory high-entropy alloys, RHEAs) demonstrated high strength up to 1600 °C but were very heavy [7,8]. Attempts to reduce their density led to the designing of RHEAs based on the (Al)-Cr-Nb-Ti-V-Zr system [9–17]. Reported alloys belonging to this system have densities, ρ, in the interval ~5.5–6.5 g/cm^3 and good specific strength up to 1000 °C [10]. Particularly, the AlNbTiV alloy with ρ = 5.59 g/cm^3 and a single phase B2 structure exhibited higher specific strength at T ≤ 800 °C in comparison with that of Inconel 718 [11,17]. Modified versions of this alloy, namely the $AlCr_xNbTiV$ and $AlNbTiVZr_x$ alloys, showed even more attractive mechanical properties in the same temperature range [13,17]. Alloying with Cr positively affects high-temperature strength, yet deteriorates ductility at ambient temperature owing to the formation of the Laves phase particles [10,13]. Certain amounts of Zr can enhance strength and ductility simultaneously due to solid solution strengthening and reducing the long-range order parameter of the B2 phase, respectively [17].

Although the effect of the chemical composition on the structure, static (mostly compression) mechanical properties, and the oxidation behavior of various RHEAs, including those belonging to the (Al)-Cr-Nb-Ti-V-Zr system, were thoroughly investigated [9,10,12,13,15,17–33], there are other properties crucial for potential applications of these alloys as high-temperature materials. One of them is the stability of structure at operating temperatures. It has already been well established that a single solid solution phase structure of (R)HEAs being stable at higher temperatures can,

* Corresponding author. Laboratory of Bulk Nanostructured Materials, Belgorod State University, Pobeda 85, Belgorod, 308015, Russia.
E-mail address: yurchenko_nikita@bsu.edu.ru (N.Yu. Yurchenko).

https://doi.org/10.1016/j.jallcom.2018.05.099
0925-8388/© 2018 Elsevier B.V. All rights reserved.

however, decompose at lower temperatures [33–43]. This change in the phase composition can have a pronounced effect on the mechanical behavior of the alloys [38]. Phase transformations can also occur in (R)HEAs with complex, multiphase microstructures [41,44]. Unfortunately, the existing information on phase transformations in RHEAs is only limited by several alloys [33,38,40–42], therefore more detailed studies are needed.

A powerful tool for the phase transformations analysis in metals and alloys is the CALPHAD (CALculations of the Phase Diagrams) method implemented in several commercial software packages [45]. The CALPHAD approach was proposed to accelerate the development of HEAs suitable for practical applications [46,47]. But in many cases, the validity of the CALPHAD predictions for HEAs remains unsatisfactory, due to limitations of the existing phase diagrams developed for conventional alloys, based on single element databases [13,15]. Commercial databases for HEAs are already available, but their accuracy requires additional verification [48,49].

Therefore in the present paper, we report the effect of a long-term (100 h) annealing at estimated operating temperatures (800–1000 °C) on the structure and mechanical properties of the refractory Al-Cr-Nb-Ti-V-Zr high entropy alloys with different Cr and Zr concentrations, namely the $AlCr_xNbTiV$ and $AlNbTiVZr_x$ ($x = 0–1.5$) alloys. Structure and mechanical properties of the alloys after high-temperature homogenization (1200 °C, 24 h) were reported elsewhere [13,17]. Note that structure of the $AlCr_xNbTiV$ ($x = 0–1.5$) alloys after compression testing at 800 °C or 1000 °C was thoroughly described in Ref. [13], however, a short-term exposure during the testing (~1.5 h) did not allow producing the equilibrium structure. The aims of the present study can be defined as follows: (i) to estimate the phase stability of the Al-Cr-Nb-Ti-V-Zr alloys depending on the Cr and Zr concentrations; (ii) to evaluate the effect of possible phase transformations on mechanical properties; (iii) to compare obtained experimental data on the phase composition of the alloys with CALPHAD predictions and to estimate their validity.

2. Experimental procedures

The alloys with a nominal composition of AlNbTiV, $AlCr_{0.5}NbTiV$ (denoted as $Cr_{0.5}$), AlCrNbTiV (Cr_1), $AlCr_{1.5}NbTiV$ ($Cr_{1.5}$), $AlNbTiVZr_{0.5}$ ($Zr_{0.5}$), AlNbTiVZr (Zr_1), and $AlNbTiVZr_{1.5}$ ($Zr_{1.5}$) were produced by arc melting of the elements in a low-pressure, high-purity argon atmosphere inside a water-cooled copper cavity. The purities of the alloying elements were no less than 99.9 at.%. The produced ingots of the alloys measured ~$6 \times 12 \times 40$ mm^3. The as-cast ingots were annealed at 1200 °C for 24 h; hereafter this condition will be referred to as the initial one. Prior to the annealing, the samples were encapsulated in vacuumed (10^{-2} torr) quartz tubes filled with titanium chips to prevent any oxidation.

Rectangular specimens measured $6 \times 4 \times 4$ mm^3 were cut using an electric discharge machine from the ingots with the initial microstructure. These specimens were then annealed at 800 °C or 1000 °C for 100 h. Prior to the annealing, the samples were also sealed in vacuumed (10^{-2} torr) quartz tubes filled with titanium chips to prevent oxidation. Then the samples were put into a preheated furnace and held for 100 h. Cooling after the annealing was carried out in laboratory air.

Microstructure and phase composition of the alloys after annealing at 800 °C or 1000 °C for 100 h were studied using X-ray diffraction (XRD), scanning electron microscopy (SEM) and transmission electron microscopy (TEM). The XRD analysis was performed using a RIGAKU diffractometer and CuKα radiation. The XRD results were used (together with TEM) for the phase identification, however, XRD patterns and lattice parameters of the constitutive phases are given in Figs. S1 and S2, and Tables S1 and S2, respectively, to avoid the excess of the graphic material. Samples for SEM observations were prepared by mechanical polishing. SEM investigations were carried out using either FEI Quanta 600 FEG or Nova NanoSEM microscopes; both instruments were equipped with back-scattered electron (BSE) and energy-dispersive X-ray spectroscopy (EDS) detectors. The volume fraction of different phases was measured by a Digimizer Image Analysis Software using SEM-BSE images. Mechanically pre-thinned to 100 μm foils were prepared for TEM analysis by conventional twinjet electro-polishing at a temperature of −35 °C and an applied voltage of 29.5 V in a mixture of 600 ml of methanol, 360 ml of butanol and 60 ml of perchloric acid. TEM investigations were performed using a JEOL JEM-2100 microscope equipped with an EDS detector at an accelerating voltage of 200 kV.

The Vickers microhardness, HV, was measured on polished cross-section surfaces of the annealed specimens using a 136-degree Vickers diamond pyramid under a 300 g load applied for 15 s. Each data point represented an average of at least 10 individual measurements. The nanohardness measurements were performed with a Shimadzu DUH-211s Dynamic Ultra Micro Hardness Tester fitted with a Berkovich tip. At least twenty indents were performed on each of the phases avoiding any influence from another phase (s). The maximum load of 50 mN was applied for 5 s; a loading speed was 6.6620 mN/s. The hardness was obtained by using the Oliver and Pharr method [50].

Isothermal compression of rectangular specimens measured $6 \times 4 \times 4$ mm^3 was carried out at 22 °C using an Instron 300LX test machine. The initial strain rate was 10^{-4} s^{-1}.

Thermodynamic modeling of equilibrium phase diagrams was conducted using a Thermo-Calc (version 2017b) software employing a TCHEA2 (High Entropy Alloys version 2.1) database.

3. Results

3.1. Structure of the Al-Cr-Nb-Ti-V-Zr alloys in the initial condition

Microstructures of the AlNbTiV, $AlCr_xNbTiV$, and $AlNbTiVZr_x$ alloys after annealing at 1200 °C for 24 h (hereinafter referred to as the initial condition) were described in details elsewhere [11,13,17]. Here, only a brief review of the relationship between the phase composition of the alloys and the Cr/Zr content is presented (Fig. 1). The AlNbTiV alloy was composed of the single B2 ordered phase [17]. Addition of a relatively small amount of Cr ($x \leq 0.5$) did not result in any visible change of the microstructure, however, at a higher Cr content the Cr_2Nb-type C14 Laves phase, enriched with Cr and Nb [13], appeared (Fig. 1a). Alloying with Zr led to the formation of the Zr_5Al_3-type phase, composed mostly of Zr and Al, at small concentrations ($0.1 \leq x \leq 0.25$), and both the Zr_5Al_3-type phase and ZrAlV-type C14 Laves phase, enriched with Zr, Al, and V, at higher ($x \geq 0.5$) content (Fig. 1b) [17]. The volume fraction of the second phases gradually enlarged with an increase in the Cr/Zr content. In all alloys, the second phase(s) particles were coarse and appeared at grain boundaries mainly rather than in the matrix (B2) grain interiors.

3.2. Effect of annealing at 800 °C or 1000 °C on microhardness of the Al-Cr-Nb-Ti-V-Zr alloys

To estimate the effect of annealing on mechanical properties of the studied alloys, microhardness measurements were performed. Fig. 2 shows the microhardness of the Al-Cr-Nb-Ti-V-Zr alloys in the initial condition and after annealings at 800 °C or 1000 °C (100 h) as a function of the Cr or Zr content. The general trend in the initial condition was an increment in the microhardness with an increase

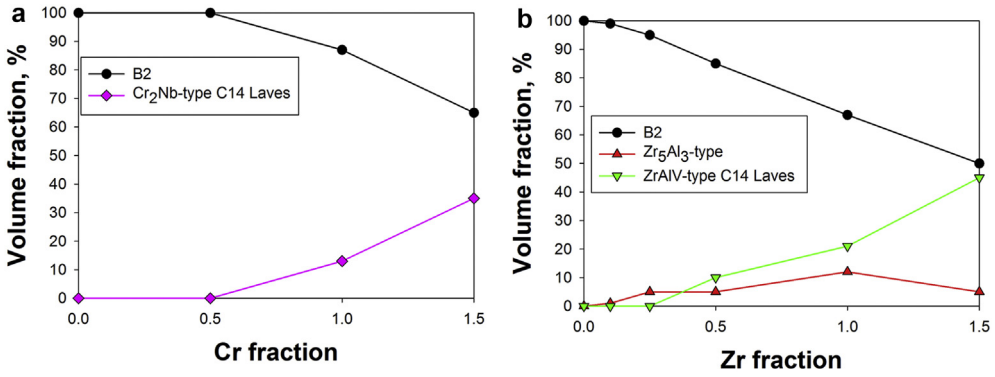

Fig. 1. Dependences of the volume fractions of the constitutive phases in the $AlCr_xNbTiV$ (a) and $AlNbTiVZr_x$ (b) alloys in the initial condition. Detailed information on the structure of the alloys can be found elsewhere [11,13,17].

in the Cr/Zr content: the microhardness raised from 450 HV for the AlNbTiV alloy to 670 HV for the $AlCr_{1.5}NbTiV$ alloy (Fig. 2a) and to 560 HV for the $AlNbTiVZr_{1.5}$ alloy (Fig. 2b). Annealings at 800 °C or 1000 °C resulted in a more complex dependence of the microhardness. The microhardness of the AlNbTiV alloy increased up to 610 HV or to 570 HV after annealing at 800 °C or 1000 °C, respectively (Fig. 2). The microhardness of the $AlCr_xNbTiV$ (x = 0.5–1.5) alloys also raised after annealing at both temperatures, yet the annealing at 800 °C led to a much higher microhardness (Fig. 2a). Also, the dependence of the microhardness on Cr fraction after annealing at 800 °C was somewhat different from that both in the initial condition or after annealing at 1000 °C. After annealing at 800 °C, the maximum hardness of 1095 HV was demonstrated by the AlCrNbTiV alloy, while further increase in the Cr concentration resulted in a lower hardness (Fig. 2a). In the $AlNbTiVZr_x$ (x = 0.5–1.5) alloys, a negligible effect of annealing at 800 °C or 1000 °C on the microhardness was found (Fig. 2b).

3.3. *Structure of the Al-Cr-Nb-Ti-V-Zr alloys after annealing at 800 °C or 1000 °C*

The AlNbTiV, $AlCr_{0.5}NbTiV$, AlCrNbTiV, $AlNbTiVZr_{0.5}$, and AlNbTiVZr alloys were chosen for detailed microstructural investigations based on the results of microhardness measurements (Fig. 2) and their microstructures in the initial condition (Fig. 1) to illustrate different kinds of behavior exhibited by the studied Al-Cr-Nb-Ti-V-Zr alloys. The microstructures of the rest of the alloys have been analyzed and are presented in Fig. S3.

Fig. 3 displays the microstructures of the AlNbTiV, $AlCr_{0.5}NbTiV$, AlCrNbTiV, $AlNbTiVZr_{0.5}$, and AlNbTiVZr alloys after annealing at 800 °C; the chemical compositions and volume fractions of the structural constituents are summarized in Table 1. The initial B2 structures of the AlNbTiV and $AlCr_{0.5}NbTiV$ alloys decomposed after annealing at 800 °C (Fig. 3a–c). The second phase appeared both along boundaries and inside B2 grains (the B2 phase marked as 1 in Fig. 3a, c) as dendritic, needle-like particles (marked as 2 in Fig. 3a, c). The second phase which can be identified as a Nb_2Al-type σ-phase (Fig. 3b) was found to be enriched with Nb and Al, and depleted of Cr (in the $AlCr_{0.5}NbTiV$ alloy) (Table 1). The volume fractions of the σ-phase in the AlNbTiV and $AlCr_{0.5}NbTiV$ alloys were 37% and 50%, respectively (Table 1); the corresponding average transversal sizes were 1.5 μm and 0.5 μm.

Annealing of the AlCrNbTiV alloy at 800 °C increased considerably the amount of the second phase(s) due to the precipitation of a great number of fine particles in the B2 matrix (Fig. 3d). Detailed analysis by TEM demonstrated that these particles were the Nb_2Al-type σ-phase enriched with Nb and Al, and depleted of Cr and V (Fig. 3e, Table 1). The volume fraction and the average size of the σ-phase were 65% (Table 1) and ~170 nm, respectively. The Cr_2Nb type C14 Laves phase particles (marked as 2 in Fig. 3d and e), composed predominantly of Cr and Nb and depleted of Ti (Table 1), retained their average transversal (~3.5 μm) and longitudinal (~8 μm) sizes and the volume fraction unchanged in comparison with those in the initial condition (Table 1 [13]).

The $AlNbTiVZr_{0.5}$ and AlNbTiVZr alloys after annealing at 800 °C were composed of the B2 matrix phase (marked as 1 in Fig. 3f and g) with the Zr_5Al_3-type (marked as 2 in Fig. 3f and g) and ZrAlV-type C14 Laves (marked as 3 in Fig. 3f and g) phases. Any other phases were not detected. The observed structures and volume fractions of the constitutive phases were very similar to those in the

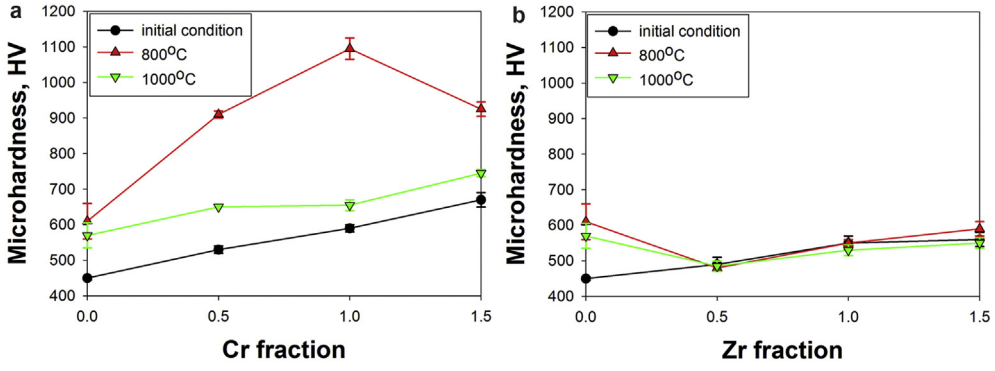

Fig. 2. Microhardness of the $AlCr_xNbTiV$ (a) and $AlNbTiVZr_x$ (b) (x = 0–1.5) alloys in the initial condition and after annealing at 800 °C or 1000 °C.

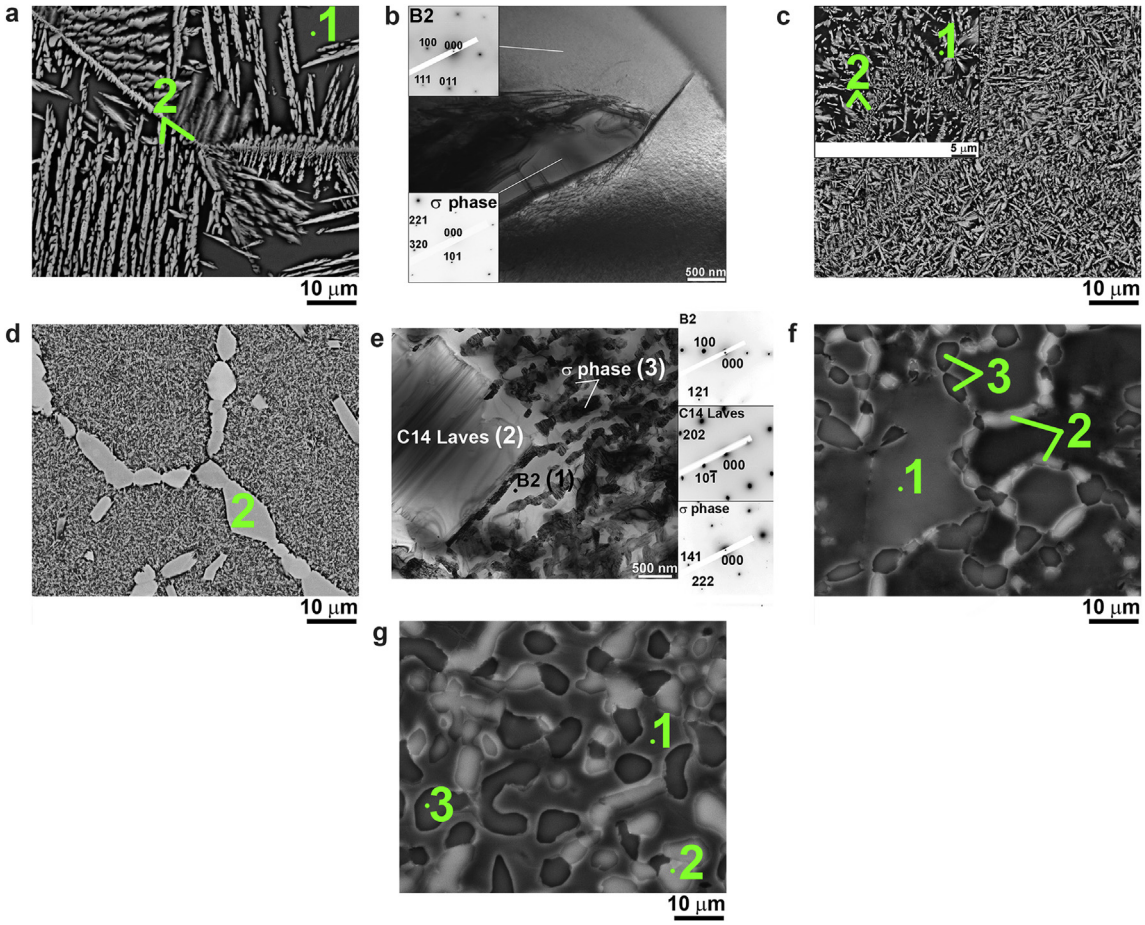

Fig. 3. SEM-BSE (a, c, d, f, g) and TEM bright-field (b, e) images of the AlNbTiV (a, b), $AlCr_{0.5}NbTiV$ (c), AlCrNbTiV (d, e), $AlNbTiVZr_{0.5}$ (f), AlNbTiVZr (g) alloys after annealing at 800 °C. Chemical compositions of the numbered structural constituents are given in Table 1.

Table 1
Chemical compositions and volume fractions of the structural constituents of the AlNbTiV, $AlCr_{0.5}NbTiV$, AlCrNbTiV, $AlNbTiVZr_{0.5}$, and AlNbTiVZr alloys after annealing at 800 °C. Analyzed areas are denoted in Fig. 3.

Elements, at.%		Al	Cr	Nb	Ti	V	Zr	Volume fraction, %
Constituents		AlNbTiV						
№	Designation							
1	B2 matrix phase	24.9	–	19.2	28.2	27.7	–	63 ± 3
2	Nb_2Al-type σ-phase	32.2	–	32.4	19.1	16.3	–	37 ± 2
Alloy composition		27.6	–	24.1	24.8	23.5	–	–
		$AlCr_{0.5}NbTiV$						
1	B2 matrix phase	22.7	11.2	19.4	23.7	23.1	–	50 ± 3
2	Nb_2Al-type σ-phase	27.3	6.6	32.4	19.6	14.3	–	50 ± 2
Alloy composition		25.2	10.3	22.3	21.4	20.8	–	–
		AlCrNbTiV						
1	B2 matrix phase	22.4	17.9	17.9	21.3	20.5	–	22 ± 3
2	Cr_2Nb-type C14 Laves phase	15.2	35.8	25.1	9.9	14.0	–	13 ± 1
3	Nb_2Al-type σ-phase	33.5	2.8	33.5	21.2	9.0	–	65 ± 3
Alloy composition		22.9	18.8	20.2	19.3	18.8	–	–
		$AlNbTiVZr_{0.5}$						
1	B2 matrix phase	21.2	–	26.3	24.6	20.6	7.3	83 ± 3
2	Zr_5Al_3-type phase	35.5	–	16.6	9.7	4.5	33.7	6 ± 2
3	ZrAlV-type C14 Laves phase	28.6	–	13.1	7.6	23.3	27.4	11 ± 2
Alloy composition		23.8	–	24.0	19.0	21.0	12.2	–
		AlNbTiVZr						
1	B2 matrix phase	16.2	–	25.9	24.9	18.3	14.7	66 ± 3
2	Zr_5Al_3-type phase	35.5	–	16.0	9.3	4.2	35.0	13 ± 2
3	ZrAlV-type C14 Laves phase	30.9	–	12.3	6.7	23.1	27.0	21 ± 2
Alloy composition		21.8	–	20.9	20.0	18.7	18.6	–

initial condition (Figs. 1 and 5 for example). The Zr_5Al_3-type phase was mostly composed of Al and Zr, while the Laves phase contained Al, V, and Zr (Table 1).

Fig. 4 illustrates the microstructures of the AlNbTiV, $AlCr_{0.5}$NbTiV and AlCrNbTiV alloys after annealing at 1000 °C; the chemical compositions and volume fractions of the structural constituents are given in Table 2. Similar to annealing at 800 °C, the initial single-phase structures of the AlNbTiV and $AlCr_{0.5}$NbTiV alloys decomposed after annealing at 1000 °C. Changes in the structure (Fig. 4a and b) were associated with the precipitation of the Nb_2Al type σ-phase (marked as 2 in Fig. 4a and b) in the matrix B2 phase (marked as 1 in Fig. 4a and b) like that observed after annealing at 800 °C (Fig. 3a, c). However, the size of the σ particles was noticeably higher in both alloys (compare Fig. 3c and Fig. 4b for example) while the volume fraction of this phase was 35% and 25% in the AlNbTiV and $AlCr_{0.5}$NbTiV alloys, respectively (Tables 1 and 2).

The AlCrNbTiV alloy after annealing at 1000 °C consisted of three constituents: the B2 phase (marked as 1 in Fig. 4c), the Cr_2Nb-type C14 Laves phase (marked as 2), and the Nb_2Al-type σ-phase (marked as 3). Although the phase composition was similar to that after annealing at 800 °C (Fig. 3d), the microstructure differed substantially. The volume fraction of the Cr_2Nb-type C14 Laves particles increased to 35% (Table 2). The Laves particles enlarged – their average transversal size increased to ~8 μm. The amount of the σ-phase (12%) was much lower than that after annealing at 800 °C (65%) (Table 2). The average size of the σ-phase particles was ~500 nm. Microstructures of the Zr-containing alloys are not presented here (but are given in Fig. S3) as they are basically identical to that after annealing at 800 °C. The chemical composition of the structural constituents of all studied alloys (Table 2) was similar to that after annealing at 800 °C.

Fig. 5 presents dependences of the volume fractions of the constitutive phases after annealings at 800 °C or 1000 °C on the Cr/Zr fractions. The most prominent change was associated with the σ-phase formation in the $AlCr_xNbTiV$ alloys (x = 0–1.5) (Fig. 5a). The volume fraction of the σ-phase demonstrated a complex dependence on the Cr concentration. After annealing at 800 °C, the amount of the σ-phase increased from 37% in the AlNbTiV alloy to 65% in the AlCrNbTiV and then lowered to 45% in the $AlCr_{1.5}$NbTiV alloy. After annealing at 1000 °C, the volume fraction of the σ-phase was maximum in the AlNbTiV alloy (35%) and decreased with an increase in the Cr fraction to ~ 1% in the $AlCr_{1.5}$NbTiV alloy (Fig. 5a). The Cr_2Nb-type C14 Laves phase was found only in the $AlCr_xNbTiV$ (x = 1; 1.5) alloys; its volume fraction was not affected significantly by annealing at 800 °C but considerably increased after annealing at 1000 °C (Figs. 1a and 5a). In the $AlNbTiVZr_x$ (x = 0.5–1.5) alloys, the volume fractions of the Zr_5Al_3-type and ZrAlV-type C14 Laves phases after annealing both at 800 °C or 1000 °C coincided with those in the initial condition (Figs. 1b and 5b).

3.4. Effect of annealing at 800 °C on mechanical properties of the Al-Cr-Nb-Ti-V-Zr alloys

Individual mechanical properties of the constitutive phases of the Al-Cr-Nb-Ti-V-Zr alloys after annealing at 800 °C for 100 h were characterized using nanoindentation (Fig. 6). In the AlNbTiV alloy, the nanohardness of the σ-phase was ~2 times higher than that of B2 phase (985 HV and 525 HV, respectively (Fig. 6a)). Due to a very fine size of the σ-phase in the $AlCr_xNbTiV$ (x = 0.5–1.5) alloys, indentation of a mixture of the B2 and σ-phases was performed.

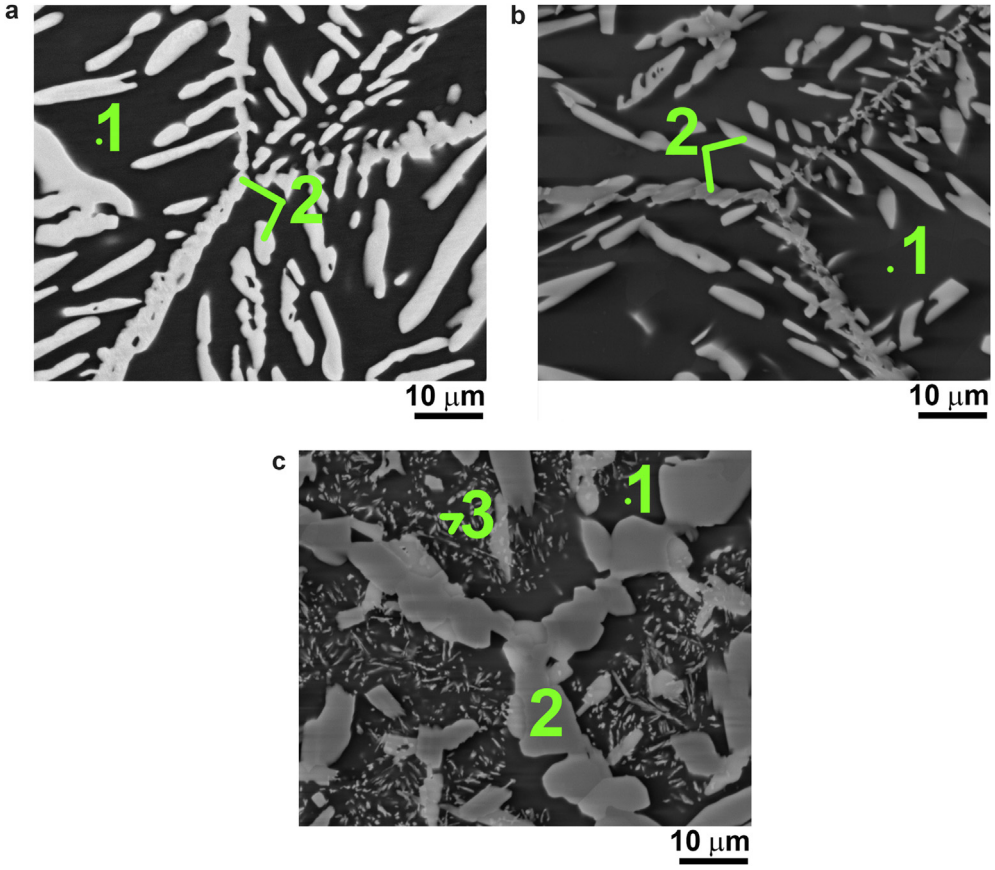

Fig. 4. SEM-BSE images of the AlNbTiV (a), $AlCr_{0.5}$NbTiV (b), AlCrNbTiV (c) alloys after annealing at 1000 °C. Chemical compositions of the numbered structural constituents are given in Table 2.

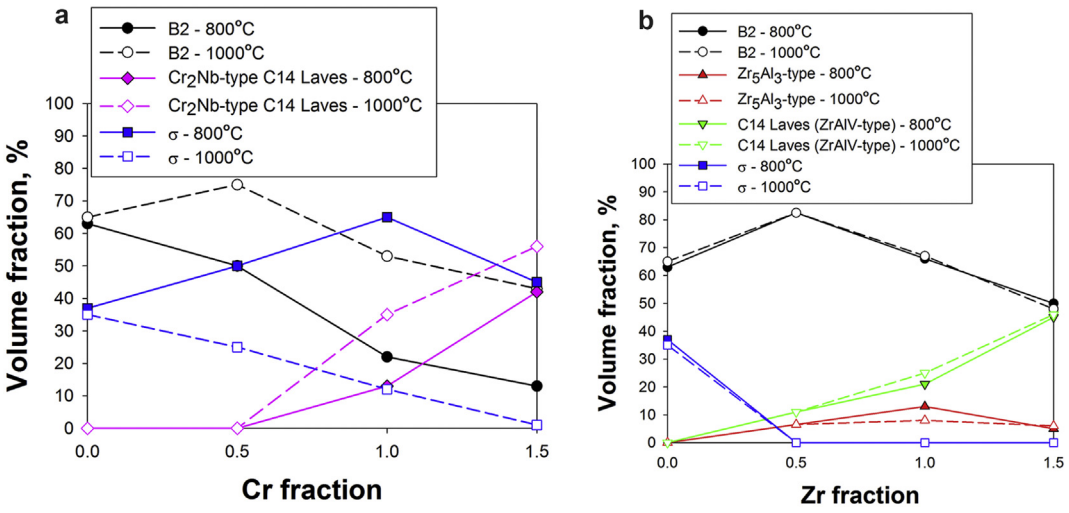

Fig. 5. Dependences of the volume fractions of the constitutive phases in the $AlCr_xNbTiV$ (a) and $AlNbTiVZr_x$ (b) (x = 0–1.5) alloys after annealing at 800 °C or 1000 °C.

Table 2
Chemical compositions and volume fractions of the structural constituents of the AlNbTiV, $AlCr_{0.5}NbTiV$ and AlCrNbTiV alloys after annealing at 1000 °C. Analyzed areas are denoted in Fig. 4.

Elements, at.%		Al	Cr	Nb	Ti	V	Zr	Volume fraction, %
Constituents		AlNbTiV						
№	Designation							
1	B2 matrix phase	24.6	–	18.8	28.7	27.9	–	65 ± 2
2	Nb_2Al-type σ-phase	31.8	–	33.3	20.3	14.6	–	35 ± 3
Alloy composition		27.6	–	24.1	24.8	23.5	–	–
		$AlCr_{0.5}NbTiV$						
1	B2 matrix phase	23.0	11.0	18.9	22.9	24.2	–	75 ± 2
2	Nb_2Al-type σ-phase	26.8	6.6	33.6	19.1	13.9	–	25 ± 2
Alloy composition		25.2	10.3	22.3	21.4	20.8	–	–
		AlCrNbTiV						
1	B2 matrix phase	22.1	18.1	18.3	20.6	20.9	–	53 ± 3
2	Cr_2Nb-type C14 Laves phase	15.4	35.6	25.5	9.7	13.8	–	35 ± 3
3	Nb_2Al-type σ-phase	33.8	2.5	33.4	21.4	8.9	–	12 ± 1
Alloy composition		22.9	18.8	20.2	19.3	18.8	–	–

Given the high hardness of the σ-phase, there is no surprise that the B2+σ mixture was much harder than the B2 phase solely (Fig. 6a). The nanohardness of the B2+σ mixture in the $AlCr_xNbTiV$ (x = 0.5–1.5) alloys increased from 1035 HV for the $AlCr_{0.5}NbTiV$ alloy to 1275 HV for the AlCrNbTiV alloy and then lowered to 1075 HV for the $AlCr_{1.5}NbTiV$ alloy (Fig. 6a).

In the $AlNbTiVZr_x$ (x = 0.5–1.5) alloys, the nanohardness of the B2 matrix showed a weak dependence on Zr content – it increased from 475 HV in the $AlNbTiVZr_{0.5}$ alloy to 515 HV in the $AlNbTiVZr_{1.5}$ alloy (Fig. 6b). Measurements of the nanohardness of the other phases, namely the Cr_2Nb-type C14 Laves phase in the $AlCr_xNbTiV$ (x = 1; 1.5) alloys, and the Zr_5Al_3-type and ZrAlV-type C14 Laves phases in the $AlNbTiVZr_x$ (x = 0.5–1.5) alloys were also performed (Fig. 6). The highest (1135–1155 HV) nanohardness was found for the Cr_2Nb-type C14 Laves phase, the lowest (800–820 HV) – for the ZrAlV-type C14 Laves phase. The Zr_5Al_3-type phase demonstrated close hardness (990–1005 HV) to that of the σ-phase (985 HV).

To evaluate the effect of annealing at 800 °C on mechanical properties of the studied alloys, room-temperature compression tests were performed. Fig. 7 illustrates engineering stress-strain curves obtained during compression of the AlNbTiV, $AlCr_{0.5}NbTiV$, AlCrNbTiV, $AlNbTiVZr_{0.5}$, and AlNbTiVZr alloys after annealing at 800 °C; corresponding mechanical properties are summarized in Table 3. Mechanical properties of the alloys in the initial condition are also shown in Table 3 for the comparison. In the AlNbTiV alloy, together with the increased yield strength, the deformation to fracture lowered from 6% in the initial condition to 0.2% after annealing at 800 °C. Both the $AlCr_{0.5}NbTiV$ and AlCrNbTiV alloys fractured in the elastic region without any plastic strain. Annealing at 800 °C decreased ductility of the $AlNbTiVZr_{0.5}$ alloy, though it retained on a reasonable level (9.8%). Ductility of the AlNbTiVZr alloy also reduced after annealing at 800 °C, but its strength properties, as well as those of the $AlNbTiVZr_{0.5}$ alloy, were very comparable with the initial ones (Fig. 7, Table 3).

3.5. Phase diagrams

Quasi-binary AlNbTiV-Cr and AlNbTiV-Zr phase diagrams constructed using the Thermo-Calc software are pictured in Fig. 8. According to Fig. 8a, the $AlCr_xNbTiV$ alloys solidified through the bcc phase. The liquidus and solidus temperatures were not significantly affected by the Cr content. The diagram predicted the precipitation of the binary Ti_3Al phase and multicomponent σ and C14 Laves phases at lower temperatures. Both the sequence of precipitation and the solvus temperatures of those phases showed a strong dependence on the Cr concentration. The Ti_3Al precipitated from the bcc phase as a primary phase at $0 \leq Cr < 0.1$; in the alloys with a higher Cr concentration it was present in multiphase (3–4 phases) fields. The solvus temperature of this phase was in a range of 680–550 °C and decreased monotonically with Cr addition. The

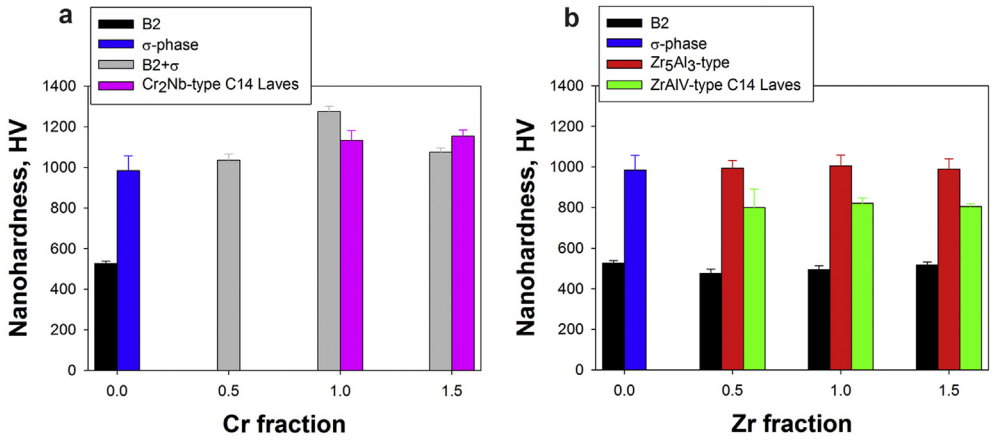

Fig. 6. Nanohardness of the constitutive phases in the $AlCr_xNbTiV$ (a) and $AlNbTiVZr_x$ (b) (x = 0–1.5) alloys after annealing at 800 °C.

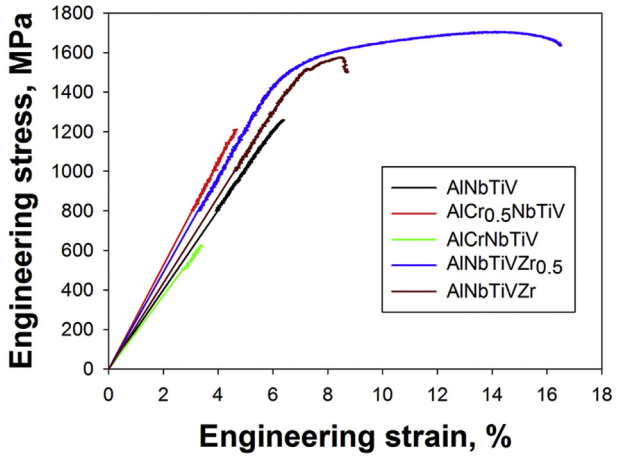

Fig. 7. Engineering stress-strain curves obtained during compression at T = 22 °C of the AlNbTiV, $AlCr_{0.5}NbTiV$, AlCrNbTiV, $AlNbTiVZr_{0.5}$, and AlNbTiVZr alloys after annealing at 800 °C.

Table 3
The room-temperature (T = 22 °C) compression yield strength (σ_{YS}), peak stress (σ_p), and fracture strain (ε) of the AlNbTiV, $AlCr_{0.5}NbTiV$, AlCrNbTiV, $AlNbTiVZr_{0.5}$, AlNbTiVZr alloys in the initial condition and after annealing at 800 °C.

Condition	Initial [11,13,17]			800 °C, 100 h		
Alloy	σ_{YS}, MPa	σ_p, MPa	ε,%	σ_{YS}, MPa	σ_p, MPa	ε,%
AlNbTiV	1000	1280	6.0	1260	1260	0.2
$AlCr_{0.5}NbTiV$	1300	1430	0.8	1210	1210	0
AlCrNbTiV	1550	1570	0.4	625	625	0
$AlNbTiVZr_{0.5}$	1485	–	>50	1445	1705	9.8
AlNbTiVZr	1500	1675	3.0	1490	1575	1.8

σ-phase, enriched with Al, Cr, and Nb, was found only in Cr-containing alloys. In the alloys with 0.1 < Cr < 0.5 the σ-phase was the first to precipitate from the primary bcc. Its solvus temperature increased first and reached the maximum (787 °C) at the Cr fraction ≈ 0.5, then fell down to ~ 630 °C at the Cr concentration = 1.5. The C14 Laves phase, enriched with Cr, Nb, and, to a lesser extent, Al, precipitated from the bcc solid solution when Cr > 0.5. The solvus temperature of the C14 Laves phase increased gradually from ~800 °C to ~1500 °C; the bcc+C14 Laves field expanded pronouncedly with an increase in the Cr concentration.

The $AlNbTiVZr_x$ alloys also solidified through the bcc phase (Fig. 8b). Contrary to Cr, Zr pronouncedly decreased both liquidus and solidus temperatures. The diagram suggested the formation of intermediate phases including the Ti_3Al and a variety of Zr_xAl_y-type phases of different stoichiometry at temperatures below ≈ 1100 °C. Similarly to the AlNbTiV-Cr diagram, the solvus temperature of the Ti_3Al phase gradually decreased from 680 °C to 500 °C when the fraction of Zr increased to ~0.75. Therefore, Ti_3Al was expected to precipitate first only in a very narrow range of Zr concentrations, from 0 to 0.5 at.%. At higher Zr concentrations, the Zr_xAl_y-type compounds appeared first. The exact stoichiometry of the compounds shifted toward higher Zr/lower Al (i.e. ZrAl → Zr_5Al_4 → Zr_4Al_3 → Zr_3Al_2) with an increase in Zr concentration in the alloys. The predicted chemical composition of the Zr_xAl_y-type compounds closely corresponded to their stoichiometric formula. The solvus temperature of the Zr-Al-rich phases raised parabolically up to ~1100 °C at Zr fraction of ~0.5 and then stagnated.

4. Discussion

4.1. Phase stability of the Al-Cr-Nb-Ti-V-Zr alloys with different Cr and Zr contents

In the present study, the stability of the initial structures of the $AlCr_xNbTiV$ and $AlNbTiVZr_x$ (x = 0–1.5) alloys after annealings at 800 °C or 1000 °C for 100 h was evaluated. In the initial condition, both Cr and Zr addition to the single B2 phase AlNbTiV alloy resulted in the formation of Cr/Zr-rich second phases; the fraction of the second phases increased in proportion to the Cr/Zr concentration (Fig. 1). However, after annealing at 800 °C or 1000 °C, the alloys demonstrated the distinctively different behavior. The structures of the $AlCr_xNbTiV$ (x = 0–1.5) alloys (including AlNbTiV alloy) were substantially affected by annealing at 800 °C or 1000 °C. The annealing response of these alloys was primarily associated with the precipitation of the Nb_2Al-type σ-phase. The amount of the σ-phase showed a complicated relationship both on Cr concentration and annealing temperature. Meanwhile, the structure of the $AlNbTiVZr_x$ (x = 0.5–1.5) alloys was barely affected by the annealings. The difference in the annealing response of the Al-Cr-Nb-Ti-V-Zr alloys with different Cr and Zr concentration is analyzed in detail below.

4.1.1. Effect of Cr

The σ-phase found in the $AlCr_xNbTiV$ (x = 0–1.5) alloys was predominantly composed of Nb and Al (Tables 1 and 2). The σ-phase of similar type after deformation/annealing at 700–1000 °C in the AlNbTiV and $AlCr_{0.5}NbTiV$ alloys has already been reported in

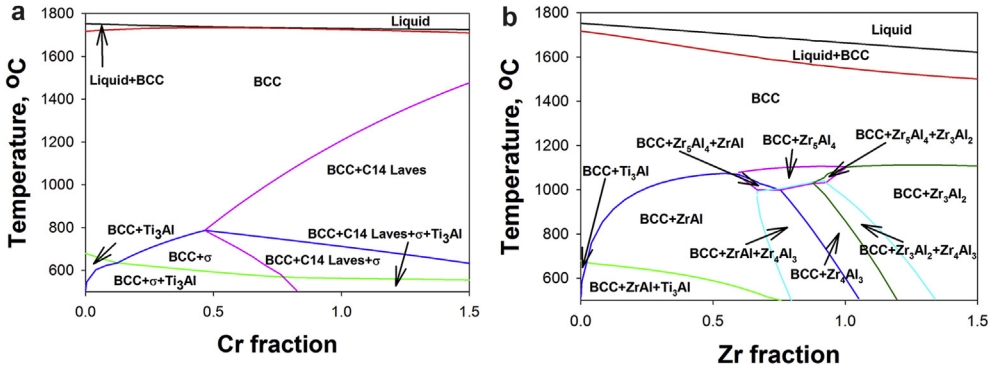

Fig. 8. Calculated quasi-binary AlNbTiV-Cr (a) and AlNbTiV-Zr (b) phase diagrams.

Refs. [13,39]. The similar phase was found in TiAlNb-based alloys: in the Ti-45Al-27Nb and Ti-45Al-22Nb-5Cr alloys with β+γ+σ structures [51] and in the Ti-45Al-22Nb-5Cr, Ti-45Al-18Nb-5Cr-1Mo, Ti-45Al-14Nb-5Cr-1Mo and Ti-45Al-18Nb alloys with γ+σ structures [52]. In the TiAlNb-based alloys, alloying with Cr was shown to reduce the transformation kinetics and the solvus temperature of the σ-phase [51], but had no effect on its volume fraction. The main factor controlling the σ-phase's amount was the Nb concentration [52]: a decrease in the Nb content led to a lower fraction of the σ-phase. In the studied $AlCr_xNbTiV$ alloys, the Nb concentration in the B2 matrix phase of the initial condition reduced with an increase in the Cr fraction [13]. It can be associated with: (i) proportional decrease in the concentration of other (than Cr) constitutive elements in the $AlCr_xNbTiV$ alloys with an increase in the Cr content; (ii) preferred segregation of Nb in the C14 Laves phase in the $AlCr_xNbTiV$ (x = 1; 1.5) alloys. Assuming that the Nb content controls the volume fraction of the σ-phase in the $AlCr_xNbTiV$ alloys, a gradual reduction in the σ-phase amount with Cr addition can be expected. Indeed, such dependence was observed after annealing at 1000 °C: the fraction of the σ-phase gradually decreased from 35% to 1% (Fig. 5a). In case of the AlCrNbTiV and $AlCr_{1.5}NbTiV$ alloys, the response to the annealing at 1000 °C was predominantly associated with an increase in the C14 Laves phase fraction (Fig. 5a) which is in reasonable agreement with the equilibrium phase diagram constructed by the Thermo-Calc software (Fig. 8a). The microstructure morphology suggests that the increase in the Laves phase fraction was mostly related to the growth of the existed particles rather than with the precipitation of new ones (Fig. 4c).

However, a more complex non-monotonic dependence of the σ-phase fraction was found after annealing at 800 °C: it increased gradually with an increase in the Cr fraction from 0 to 1 and then decreased slightly (Fig. 5a). Also note, that contrary to the annealing at 1000 °C, the fraction of the Laves phase in the AlCrNbTiV and $AlCr_{1.5}NbTiV$ alloys was not affected significantly. Complex changes of the constitutive phases' fractions can be expected in the alloys with three-phase fields in phase diagrams. For example, the dependences of a fraction of constitutive phases in the $AlCr_{0.5}NbTiV$, AlCrNbTiV, and $AlCr_{1.5}NbTiV$ alloys on temperature (constructed by the Thermo-Calc) is shown in Fig. 9. One can clearly see that at temperatures below 600 °C the fractions of the σ-phase in the $AlCr_{0.5}NbTiV$ and AlCrNbTiV alloys are nearly equal, whereas the σ-phase fraction in the $AlCr_{1.5}NbTiV$ alloy is considerably lower than in the first two alloys. This result is in reasonable agreement with the experimental data for the $AlCr_xNbTiV$ (x = 0.5–1.5) alloys after annealing at 800 °C.

Moreover, in the AlCrNbTiV and $AlCr_{1.5}NbTiV$ alloys in the two-phase field (bcc+Laves) a decrease in temperature results in a continuous increase in the Laves phase fraction (Fig. 9b and c). However, in the three-phase field (bcc+Laves+σ) the fraction of the bcc and Laves phases decreases continuously while the σ-phase fraction increases. That is most probably why the annealing at 800 °C resulted in the precipitation of the σ-phase particles but the fraction of the Laves phase almost did not change in comparison with the initial condition.

But, although the Thermo-Calc describes the phase equilibria in the AlNbTiV-Cr alloys rather suitably, details of the produced phase diagrams are mostly incorrect. For example, the experimental data suggest that the solvus temperature of the σ-phase in the studied $AlCr_xNbTiV$ (x = 0–1.5) alloys is within the interval of 1000–1200 °C, whereas the predicted σ-phase had the maximum solvus temperature of 787 °C. Moreover, according to the calculations, the σ-phase precipitation does not occur in the AlNbTiV alloy at temperatures above 500 °C, and the chemical composition of the experimentally observed phase significantly differs from that of the predicted one (the predicted phase is expected to be Cr-rich, while the experimental one is almost free of Cr (Tables 1 and 2)). These inaccuracies can possibly be attributed to the absence of the ternary Al-Nb-Ti diagram in the TCHEA2 database [53]. Among the constitutive ternaries of the Al-Nb-Ti-V system, only the Al-Nb-Ti contains a description of the Nb_2Al-type σ-phase [54]. In addition, the matrix bcc phase in the initial condition is predicted to be disordered, while the experimental matrix phase has the B2 ordered structure.

4.1.2. *Effect of Zr*

The Zr-containing alloys were different from the AlNbTiV and its Cr-containing variants in (i) absence of the σ-phase after annealing at 800 °C or 1000 °C and (ii) very small variation in the fraction of constitutive phases (Figs. 1 and 5b). The role of Zr in the preventing the σ-phase appearance most likely originates from a firm tendency to form its own very stable compounds. For instance, Wen et al. [55] reported that a small Zr addition can inhibit the σ-phase in a stainless steel during a long-term aging due to the preferable formation of a ZrC-carbide instead of a G-phase which serves as a nucleation site for the σ-phase. In our case, Zr apparently suppressed the Nb_2Al-type σ-phase due to higher than Nb affinity to Al [56,57] by trapping Al into ZrAl-rich phases, namely Zr_5Al_3-type and ZrAlV-type C14 Laves, which had formed in the initial condition (Fig. 1b).

Meanwhile, the Zr_5Al_3-type and ZrAlV-type C14 Laves phases were almost unaffected by the annealing at 800 °C or 1000 °C. The presented data show that the phase composition of the $AlNbTiVZr_x$ (x = 0.5–1.5 alloys) is insensitive to annealing at temperatures in the range of 800–1200 °C, however strongly depends on the Zr content. Such behavior can be anticipated from the AlNbTiV-Zr

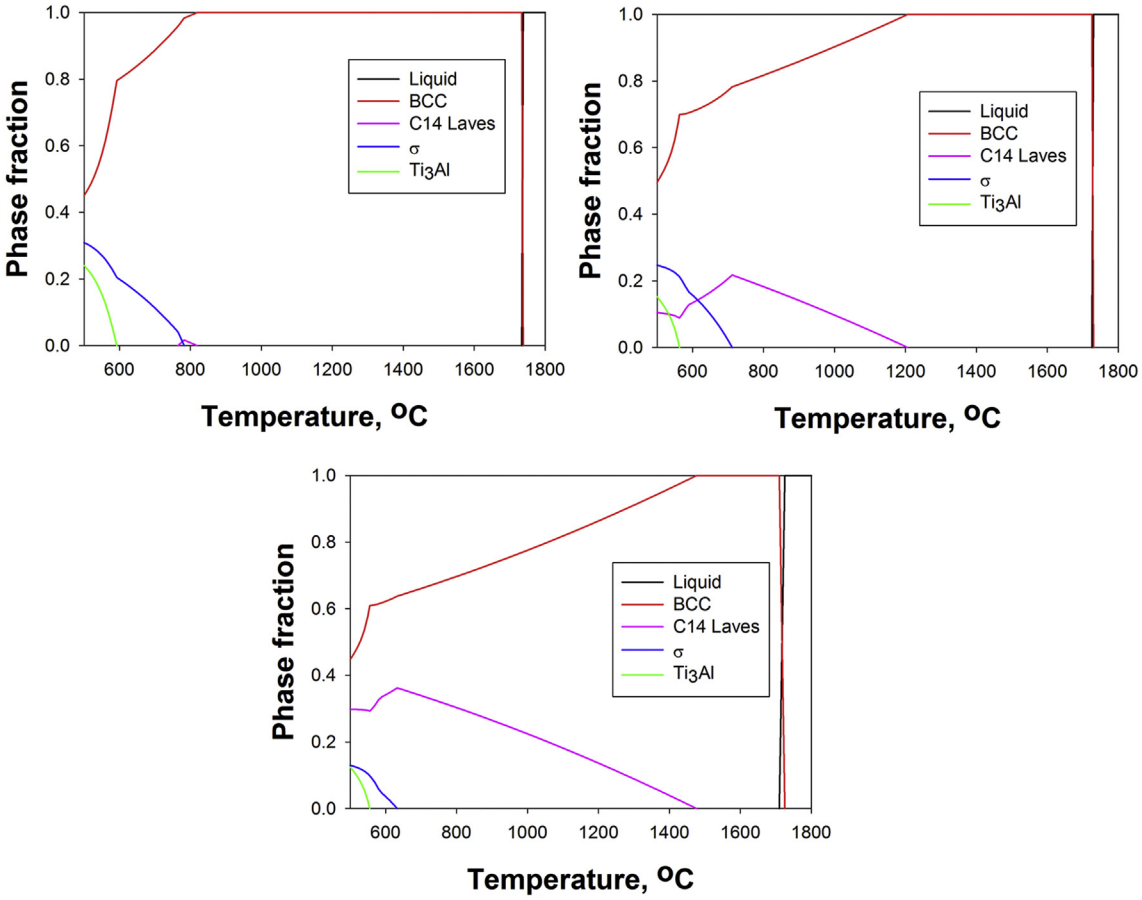

Fig. 9. Dependence of the fraction of the equilibrium phases on temperature obtained using the Thermo-Calc software in the $AlCr_{0.5}NbTiV$ alloy (a); AlCrNbTiV alloy (b); $AlCr_{1.5}NbTiV$ alloy (c).

phase diagram (Fig. 8b). The relatively rapid growth of the solvus temperature of the second phases with an increase in the molar fraction of Zr to ≈0.5 and a nearly constant solvus temperature of the second phases in the alloys with a higher Zr fraction implies the relative stability of the phase composition of the $AlNbTiVZr_x$ (x = 0.5–1.5) alloys in the multi-phase fields.

However, the constructed AlNbTiV-Zr phase diagram incorrectly predicts many aspects of the phase equilibria in the $AlNbTiVZr_x$ (x = 0.5–1.5) alloys. For instance, the solvus temperature of the second phases, according to the experimental data, is above 1200 °C, while the predicted solvus temperature is ≈ 1100 °C. The predicted type of the second phases is also incorrect; the Zr_5Al_3-type and ZrAlV-type C14 Laves phases were found instead of Zr_xAl_y-type phases of different stoichiometry. Partially, this discrepancy can be attributed to an incorrect assessment of the homogeneity range of the Zr_5Al_3-type phase. The predicted phase has a nearly stoichiometric composition while the experimental one contains ~30 at.% (in total) of Nb, Ti, and V (Table 1). Also, the addition of Zr mostly results in the formation of the C14 Laves phase (Figs. 1b and 5b) that is not predicted by the Thermo-Calc most probably due to limitations of the commercial database used in this study.

Integrally, the comparison between the predicted AlNbTiV-Cr and AlNbTiV-Zr phase diagrams and the experimental data on phase composition of the $AlCr_xNbTiV$ and $AlNbTiVZr_x$ (x = 0–1.5) alloys demonstrated that although the Thermo-Calc predictions give right ideas about phase equilibria and transformations in general, the accurate assessment of the solvus temperatures, type of phases, their chemical compositions and fractions in the Al-Cr-Nb-Ti-V-Zr alloys using the available commercial database for high-entropy alloys is impossible at the moment.

4.2. Effect of annealing on mechanical properties of the Al-Cr-Nb-Ti-V-Zr alloys

The effect of annealing on mechanical properties of the AlNbTiV-based alloys with Cr and Zr is significantly different (Figs. 2 and 7, Table 3). The microhardness of the $AlCr_xNbTiV$ (x = 0–1.5) alloys, including the AlNbTiV alloy, pronouncedly increased after annealing at 800 °C (Fig. 2a), whereas hardness of the $AlNbTiVZr_x$ (x = 0.5–1.5) alloys was barely affected (Fig. 2b). The difference in the microhardness can be possibly associated with the changes in phase compositions of the alloys upon annealing. Quantitative estimation of the effect of phase compositions of the studied alloys on their hardness can be done using the rule of a mixture (ROM) [13]. As the volume fraction and hardness of each phase are known for samples annealed at 800 °C, the following formula can be used:

$$HV_{overall} = \Big(V_{B2}{*}HV_{B2} + V_{\sigma}{*}HV_{\sigma} + V_{B2+\sigma}{*}HV_{B2+\sigma} + V_{Laves(Cr2Nb)}{*}HV_{Laves(Cr2Nb)} + V_{Zr5Al3}{*}HV_{Zr5Al3} + V_{Laves(ZrAlV)}{*}HV_{Laves(ZrAlV)}\Big){*}k \quad (1)$$

where V_{B2}, V_{σ}, $V_{B2+\sigma}$, $V_{Laves(Cr2Nb)}$, V_{Zr5Al3}, and $V_{Laves(ZrAlV)}$ are the volume fractions of the B2, σ, B2+σ mixture, Cr_2Nb-type C14 Laves,

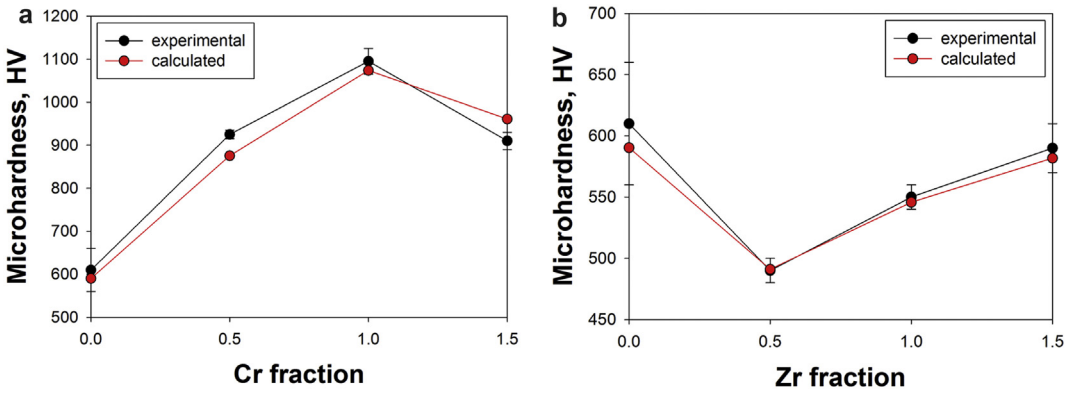

Fig. 10. Comparison between experimental and calculated microhardness of the $AlCr_xNbTiV$ (a) and $AlNbTiVZr_x$ (b) alloys after annealing at 800 °C.

Zr_5Al_3-type, and ZrAlV-type C14 Laves phases, respectively, taken from Table 1 and data pictured in Fig. 5; HV_{B2}, HV_{σ}, $HV_{B2+\sigma}$, $HV_{Laves(Cr2Nb)}$, HV_{Zr5Al3}, and $HV_{Laves(ZrAlV)}$ are the nanohardnesses of the corresponding phases and the following values were used for the calculations: $HV_{B2} = 515$ HV; $HV_{\sigma} = 1000$ HV; $HV_{B2+\sigma} = 1030$ HV ($AlCr_{0.5}NbTiV$), 1280 HV (AlCrNbTiV), 1080 HV ($AlCr_{1.5}NbTiV$); $HV_{Laves(Cr2Nb)} = 1150$ HV; $HV_{Zr5Al3} = 1000$ HV; $HV_{Laves(ZrAlV)} = 820$ HV; k – the correction factor calculated as a ratio between the microhardness and nanohardness values of the B2 phase in the AlNbTiV alloy in the initial condition (Fig. 1), equals to 0.85. Note that the measurements of the nanohardness of individual phases in the fine B2+σ mixture in the $AlCr_xNbTiV$ (x = 0.5–1.5) alloys was impossible and therefore nanohardness of the B2+σ mixture was used.

The hardness values, calculated using equation (1), are in good agreement with the experimental data (Fig. 10). A good correlation between the experimental hardness and ROM predictions indicates that the increase in the hardness in the $AlCr_xNbTiV$ (x = 0–1.5) alloys is associated with the precipitation of the hard σ-phase. The higher fraction of the σ-phase in the $AlCr_xNbTiV$ (x = 0–1.5) alloys after annealing at 800 °C is likely to be the reason of the higher hardness in comparison with that after annealing at 1000 °C (Figs. 2 and 5a). Note that the increase in the Laves phase fraction in the AlCrNbTiV and $AlCr_{1.5}NbTiV$ alloys after annealing at 1000 °C should also contribute to hardening. Meanwhile, the hardness of the $AlNbTiVZr_x$ (x = 0.5–1.5) alloys is weakly affected by the annealing because of stability of their microstructure.

The compression tests have also revealed a considerable effect of the annealing at 800 °C on mechanical properties of the alloys (Fig. 7, Table 3). These changes were primarily associated with ductility of the alloys rather than their strength. For instance, the ductility of the AlNbTiV alloy dropped from 6% to 0.2% after annealing. Apparently, such pronounced embrittlement is due to the precipitation of a large amount of the σ-phase particles [58]. The σ-phase is well known for its brittleness [59]. At the same time, the regions containing the σ-phase are likely not to be actively involved in plastic deformation; therefore the yield strength showed only a moderate increase (1260 MPa vs 1000 MPa). The $AlCr_{0.5}NbTiV$ and AlCrNbTiV alloys fractured in the elastic region, most probably due to the even higher amount of the fine σ precipitates that can limit the capacity of plastic deformation of the B2 matrix (Fig. 3). The very low yield strength of the AlCrNbTiV alloy after annealing is likely the result of the premature fracture even in compression due to the extreme brittleness of the alloy composed mostly of intermetallic phases (Fig. 5a).

The absence of significant changes in the phase composition of the $AlNbTiVZr_x$ (x = 0.5–1.5) alloys suggests stability of the mechanical properties. Indeed, the annealing at 800 °C barely affects the yield strength of the $AlNbTiVZr_{0.5}$ and AlNbTiVZr alloys (Table 3). But, although the annealed $AlNbTiVZr_{0.5}$ alloy demonstrated reasonable compression ductility of 9.8%, it is much lower than that in the initial condition [14]. Ductility of the AlNbTiVZr also decreased after annealing. The reasons of the reduced ductility of the alloys are unclear at the moment; apparently, it cannot be associated with the small changes in the phase composition after annealing (compare Figs. 1 and 5b). Probably, annealing can result in changes of the long-range order parameter of the B2 phase which was recently found to have a decisive effect on the ductility of the $AlNbTiVZr_x$ alloys [17]. However, further studies are required to verify this assumption.

To sum up, the relative stability of the microstructure and mechanical properties of the $AlNbTiVZr_x$ (x = 0.5–1.5 alloys) after annealing at temperatures of 800 °C or 1000 °C together with high strength at temperatures up to 800 °C [17] confirm their potential as high-temperature materials. At the same time, the $AlCr_xNbTiV$ (x = 0–1.5) alloys suffer from the precipitation of the σ-phase and drastic embrittlement after annealing. This behavior may limit their potential applications despite impressive high-temperature strength [13].

5. Conclusions

In this study the effect of annealing at 800 °C or 1000 °C for 100 h on the initial structure and mechanical properties of the refractory Al-Cr-Nb-Ti-V-Zr high-entropy alloys with different Cr and Zr concentrations was studied and following conclusions were drawn:

1) In the initial condition (annealing at 1200 °C for 24 h), the AlNbTiV and $AlCr_{0.5}NbTiV$ alloys were composed of the B2 phase while the AlCrNbTiV and $AlCr_{1.5}NbTiV$ alloys had the B2 and Cr_2Nb-type C14 Laves phases. Annealing at 800 °C or 1000 °C resulted in the precipitation of the Nb_2Al-type σ-phase, enriched with Nb and Al, and an increase in the fraction of the Laves phase in the AlCrNbTiV and $AlCr_{1.5}NbTiV$ alloys at 1000 °C.
2) The $AlNbTiVZr_x$ (x = 0.5–1.5) alloys in the initial condition consisted of the B2, Zr_5Al_3-type, and ZrAlV-type C14 Laves phases. The fraction of the second phases increased with an increase in the Zr content. Annealing at 800 °C or 1000 °C led to insignificant changes in the volume fraction of the constitutive phases.
3) Equilibrium quasi-binary AlNbTiV-Cr and AlNbTiV-Zr phase diagrams were constructed using the Thermo-Calc software and the TCHEA2 database. The comparison between the Thermo-

Calc predictions and the experimental data showed that rough predictions of the phase equilibria in the studied Al-Cr-Nb-Ti-V-Zr alloys can be made using the commercial software and database, whereas the predicted phase transformation temperatures, types and chemical compositions of constitutive phases are generally incorrect.

4) Annealing of the $AlCr_xNbTiV$ ($x = 0–1.5$) alloys at 800 °C or 1000 °C led to an increase in the microhardness. The highest value, 1095 HV, was demonstrated by the AlCrNbTiV alloy after annealing at 800 °C. It was revealed that hardening of the alloys was associated with the precipitation of the σ-phase. The microhardness of the $AlNbTiVZr_x$ ($x = 0.5–1.5$) alloys was not affected by the annealing.
5) Annealing at 800 °C pronouncedly affected compression ductility of the studied alloys. Ductility of the AlNbTiV, $AlCr_{0.5}NbTiV$, and AlCrNbTiV alloys dropped to 0–0.2%. The strong decrease in ductility was associated with the precipitation of the brittle σ-phase. Ductility of the $AlNbTiVZr_{0.5}$ and AlNbTiVZr alloys also decreased, for instance, compression ductility of the $AlNbTiVZr_{0.5}$ alloy was >50% and 9.8% in the initial condition and after annealing at 800 °C, respectively.

Acknowledgments

The authors gratefully acknowledge the financial support from the Russian Science Foundation (Grant No. 14-19-01104). The authors are grateful to the personnel of the Joint Research Center, «Technology and Materials», Belgorod State National Research University, for their assistance with the instrumental analysis. The authors are also grateful to Dr. M.A. Tikhonovsky for supplying the ingots of the investigated alloys.

Appendix A. Supplementary data

Supplementary data related to this article can be found at https://doi.org/10.1016/j.jallcom.2018.05.099.

References

[1] J.W. Yeh, S.K. Chen, S.J. Lin, J.Y. Gan, T.S. Chin, T.T. Shun, C.H. Tsau, S.Y. Chang, Nanostructured high-entropy alloys with multiple principal elements: novel alloy design concepts and outcomes, Adv. Eng. Mater. 6 (2004), https://doi.org/10.1002/adem.200300567, 299–303+274.
[2] Y. Zhang, T.T. Zuo, Z. Tang, M.C. Gao, K.A. Dahmen, P.K. Liaw, Z.P. Lu, Microstructures and properties of high-entropy alloys, Prog. Mater. Sci. 61 (2014) 1–93, https://doi.org/10.1016/j.pmatsci.2013.10.001.
[3] M.-H. Tsai, J.-W. Yeh, High-entropy alloys: a critical review, Mater. Res. Lett. 2 (2014) 107–123, https://doi.org/10.1080/21663831.2014.912690.
[4] D.B. Miracle, O.N. Senkov, A critical review of high entropy alloys and related concepts, Acta Mater. 122 (2017) 448–511, https://doi.org/10.1016/j.actamat.2016.08.081.
[5] A.D. Pogrebnjak, A.A. Bagdasaryan, I.V. Yakushchenko, V.M. Beresnev, The structure and properties of high-entropy alloys and nitride coatings based on them, Russ. Chem. Rev. 83 (2014) 1027–1061, https://doi.org/10.1070/RCR4407.
[6] S. Gorsse, D.B. Miracle, O.N. Senkov, Mapping the world of complex concentrated alloys, Acta Mater. 135 (2017) 177–187, https://doi.org/10.1016/j.actamat.2017.06.027.
[7] O.N. Senkov, G.B. Wilks, D.B. Miracle, C.P. Chuang, P.K. Liaw, Refractory high-entropy alloys, Intermetallics 18 (2010) 1758–1765, https://doi.org/10.1016/j.intermet.2010.05.014.
[8] O.N. Senkov, G.B. Wilks, J.M. Scott, D.B. Miracle, Mechanical properties of $Nb_{25}Mo_{25}Ta_{25}W_{25}$ and $V_{20}Nb_{20}Mo_{20}Ta_{20}W_{20}$ refractory high entropy alloys, Intermetallics 19 (2011) 698–706, https://doi.org/10.1016/j.intermet.2011.01.004.
[9] O.N. Senkov, S.V. Senkova, C. Woodward, D.B. Miracle, Low-density, refractory multi-principal element alloys of the Cr-Nb-Ti-V-Zr system: microstructure and phase analysis, Acta Mater. 61 (2013) 1545–1557, https://doi.org/10.1016/j.actamat.2012.11.032.
[10] O.N. Senkov, S.V. Senkova, D.B. Miracle, C. Woodward, Mechanical properties of low-density, refractory multi-principal element alloys of the Cr–Nb–Ti–V–Zr system, Mater. Sci. Eng. A 565 (2013) 51–62, https://doi.org/10.1016/j.msea.2012.12.018.
[11] N.D. Stepanov, D.G. Shaysultanov, G.A. Salishchev, M.A. Tikhonovsky, Structure and mechanical properties of a light-weight AlNbTiV high entropy alloy, Mater. Lett. 142 (2015) 153–155, https://doi.org/10.1016/j.matlet.2014.11.162.
[12] N.D. Stepanov, N. Yu Yurchenko, D.G. Shaysultanov, G.A. Salishchev, M.A. Tikhonovsky, Effect of Al on structure and mechanical properties of $Al_xNbTiVZr$ ($x = 0, 0.5, 1, 1.5$) high entropy alloys, Mater. Sci. Technol. 31 (2015), https://doi.org/10.1179/1743284715Y.0000000032 (United Kingdom).
[13] N.D. Stepanov, N.Y. Yurchenko, D.V. Skibin, M.A. Tikhonovsky, G.A. Salishchev, Structure and mechanical properties of the $AlCr_xNbTiV$ ($x = 0, 0.5, 1, 1.5$) high entropy alloys, J. Alloys Compd. 652 (2015) 266–280, https://doi.org/10.1016/j.jallcom.2015.08.224.
[14] N.D. Stepanov, N.Y. Yurchenko, V.S. Sokolovsky, M.A. Tikhonovsky, G.A. Salishchev, An $AlNbTiVZr_{0.5}$ high-entropy alloy combining high specific strength and good ductility, Mater. Lett. 161 (2015) 136–139, https://doi.org/10.1016/j.matlet.2015.08.099.
[15] N.Y. Yurchenko, N.D. Stepanov, D.G. Shaysultanov, M.A. Tikhonovsky, G.A. Salishchev, Effect of Al content on structure and mechanical properties of the $Al_xCrNbTiVZr$ ($x = 0; 0.25; 0.5; 1$) high-entropy alloys, Mater. Char. 121 (2016), https://doi.org/10.1016/j.matchar.2016.09.039.
[16] N.D. Stepanov, N.Y. Yurchenko, E.S. Panina, M.A. Tikhonovsky, S.V. Zherebtsov, Precipitation-strengthened refractory $Al_{0.5}CrNbTi_2V_{0.5}$ high entropy alloy, Mater. Lett. 188 (2017), https://doi.org/10.1016/j.matlet.2016.11.030.
[17] N.Y. Yurchenko, N.D. Stepanov, S.V. Zherebtsov, M.A. Tikhonovsky, G.A. Salishchev, Structure and mechanical properties of B2 ordered refractory $AlNbTiVZr_x$ ($x = 0–1.5$) high-entropy alloys, Mater. Sci. Eng. A 704 (2017) 82–90, https://doi.org/10.1016/j.msea.2017.08.019.
[18] B. Ren, Z. Shen, Z. Liu, Structure and mechanical properties of multi-element $(AlCrMnMoNiZr)N_x$ coatings by reactive magnetron sputtering, J. Alloys Compd. 560 (2013) 171–176, https://doi.org/10.1016/J.JALLCOM.2013.01.148.
[19] A.D. Pogrebnjak, I.V. Yakushchenko, O.V. Bondar, V.M. Beresnev, K. Oyoshi, O.M. Ivasishin, H. Amekura, Y. Takeda, M. Opielak, C. Kozak, Irradiation resistance, microstructure and mechanical properties of nanostructured (TiZrHfVNbTa)N coatings, J. Alloys Compd. 679 (2016) 155–163, https://doi.org/10.1016/J.JALLCOM.2016.04.064.
[20] T.M. Butler, K.J. Chaput, J.R. Dietrich, O.N. Senkov, High temperature oxidation behaviors of equimolar NbTiZrV and NbTiZrCr refractory complex concentrated alloys (RCCAs), J. Alloys Compd. 729 (2017) 1004–1019, https://doi.org/10.1016/j.jallcom.2017.09.164.
[21] N.N. Guo, L. Wang, L.S. Luo, X.Z. Li, Y.Q. Su, J.J. Guo, H.Z. Fu, Microstructure and mechanical properties of refractory MoNbHfZrTi high-entropy alloy, Mater. Des. 81 (2015) 87–94, https://doi.org/10.1016/j.matdes.2015.05.019.
[22] C.C. Juan, M.H. Tsai, C.W. Tsai, C.M. Lin, W.R. Wang, C.C. Yang, S.K. Chen, S.J. Lin, J.W. Yeh, Enhanced mechanical properties of HfMoTaTiZr and HfMoNbTaTiZr refractory high-entropy alloys, Intermetallics 62 (2015) 76–83, https://doi.org/10.1016/j.intermet.2015.03.013.
[23] C.M. Lin, C.C. Juan, C.H. Chang, C.W. Tsai, J.W. Yeh, Effect of Al addition on mechanical properties and microstructure of refractory $Al_xHfNbTaTiZr$ alloys, J. Alloys Compd. 624 (2015) 100–107, https://doi.org/10.1016/j.jallcom.2014.11.064.
[24] C.-C. Juan, K.-K. Tseng, W.-L. Hsu, M.-H. Tsai, C.-W. Tsai, C.-M. Lin, S.-K. Chen, S.-J. Lin, J.-W. Yeh, Solution strengthening of ductile refractory $HfMo_xNbTaTiZr$ high-entropy alloys, Mater. Lett. 175 (2016) 284–287, https://doi.org/10.1016/J.MATLET.2016.03.133.
[25] H.W. Yao, J.W. Qiao, J.A. Hawk, H.F. Zhou, M.W. Chen, M.C. Gao, Mechanical properties of refractory high-entropy alloys: experiments and modeling, J. Alloys Compd. 696 (2017) 1139–1150, https://doi.org/10.1016/J.JALLCOM.2016.11.188.
[26] Z.D. Han, N. Chen, S.F. Zhao, L.W. Fan, G.N. Yang, Y. Shao, K.F. Yao, Effect of Ti additions on mechanical properties of NbMoTaW and VNbMoTaW refractory high entropy alloys, Intermetallics 84 (2017) 153–157, https://doi.org/10.1016/J.INTERMET.2017.01.007.
[27] Z.D. Han, H.W. Luan, X. Liu, N. Chen, X.Y. Li, Y. Shao, K.F. Yao, Microstructures and mechanical properties of $Ti_xNbMoTaW$ refractory high-entropy alloys, Mater. Sci. Eng. A 712 (2018) 380–385, https://doi.org/10.1016/J.MSEA.2017.12.004.
[28] B. Gorr, M. Azim, H.J. Christ, T. Mueller, D. Schliephake, M. Heilmaier, Phase equilibria, microstructure, and high temperature oxidation resistance of novel refractory high-entropy alloys, J. Alloys Compd. 624 (2015) 270–278, https://doi.org/10.1016/j.jallcom.2014.11.012.
[29] H. Chen, A. Kauffmann, B. Gorr, D. Schliephake, C. Seemüller, J.N. Wagner, H.J. Christ, M. Heilmaier, Microstructure and mechanical properties at elevated temperatures of a new Al-containing refractory high-entropy alloy Nb-Mo-Cr-Ti-Al, J. Alloys Compd. 661 (2016) 206–215, https://doi.org/10.1016/j.jallcom.2015.11.050.
[30] B. Gorr, F. Müller, M. Azim, H.-J. Christ, T. Müller, H. Chen, A. Kauffmann, M. Heilmaier, High-temperature oxidation behavior of refractory high-entropy alloys: effect of alloy composition, Oxid. Met. (2017) 1–11, https://doi.org/10.1007/s11085-016-9696-y.
[31] S. Sheikh, S. Shafeie, Q. Hu, J. Ahlström, C. Persson, J. Veselý, J. Zýka, U. Klement, S. Guo, Alloy design for intrinsically ductile refractory high-entropy alloys, J. Appl. Phys. 120 (2016), 164902, https://doi.org/10.1063/1.4966659.
[32] S. Sheikh, M.K. Bijaksana, A. Motallebzadeh, S. Shafeie, A. Lozinko, L. Gan, T.-K. Tsao, U. Klement, D. Canadinc, H. Murakami, S. Guo, Accelerated oxidation

in ductile refractory high-entropy alloys, Intermetallics 97 (2018) 58–66, https://doi.org/10.1016/J.INTERMET.2018.04.001.
[33] Y. Wu, J. Si, D. Lin, T. Wang, W.Y. Wang, Y. Wang, Z. Liu, X. Hui, Phase stability and mechanical properties of AlHfNbTiZr high-entropy alloys, Mater. Sci. Eng. A 724 (2018) 249–259, https://doi.org/10.1016/J.MSEA.2018.03.071.
[34] E.J. Pickering, R. Muñoz-Moreno, H.J. Stone, N.G. Jones, Precipitation in the equiatomic high-entropy alloy CrMnFeCoNi, Scr. Mater. 113 (2016) 106–109, https://doi.org/10.1016/j.scriptamat.2015.10.025.
[35] F. Otto, A. Dlouhý, K.G. Pradeep, M. Kuběnová, D. Raabe, G. Eggeler, E.P. George, Decomposition of the single-phase high-entropy alloy CrMnFeCoNi after prolonged anneals at intermediate temperatures, Acta Mater. 112 (2016) 40–52, https://doi.org/10.1016/j.actamat.2016.04.005.
[36] F. He, Z. Wang, Q. Wu, J. Li, J. Wang, C.T. Liu, Phase separation of metastable CoCrFeNi high entropy alloy at intermediate temperatures, Scr. Mater. 126 (2017) 15–19, https://doi.org/10.1016/j.scriptamat.2016.08.008.
[37] N.D. Stepanov, D.G. Shaysultanov, M.S. Ozerov, S.V. Zherebtsov, G.A. Salishchev, Second phase formation in the CoCrFeNiMn high entropy alloy after recrystallization annealing, Mater. Lett. 185 (2016) 1–4, https://doi.org/10.1016/j.matlet.2016.08.088.
[38] N.D. Stepanov, N.Y. Yurchenko, S.V. Zherebtsov, M.A. Tikhonovsky, G.A. Salishchev, Aging behavior of the HfNbTaTiZr high entropy alloy, Mater. Lett. 211 (2017), https://doi.org/10.1016/j.matlet.2017.09.094.
[39] B. Schuh, B. Völker, V. Maier-Kiener, J. Todt, J. Li, A. Hohenwarter, Phase decomposition of a single-phase AlTiVNb high-entropy alloy after severe plastic deformation and Annealing , Adv. Eng. Mater. (2017), 1600674 https://doi.org/10.1002/adem.201600674.
[40] O.N. Senkov, S.L. Semiatin, Microstructure and properties of a refractory high-entropy alloy after cold working, J. Alloys Compd. 649 (2015) 1110–1123, https://doi.org/10.1016/j.jallcom.2015.07.209.
[41] N.Y. Yurchenko, N.D. Stepanov, M.A. Tikhonovsky, G.A. Salishchev, Phase evolution of the $Al_xNbTiVZr$ (x = 0; 0.5; 1; 1.5) high entropy alloys, Metals vol. 6 (2016), https://doi.org/10.3390/met6120298 (Basel).
[42] B. Schuh, B. Völker, J. Todt, N. Schell, L. Perrière, J. Li, J.P. Couzinié, A. Hohenwarter, Thermodynamic instability of a nanocrystalline, single-phase TiZrNbHfTa alloy and its impact on the mechanical properties, Acta Mater. 142 (2018) 201–212, https://doi.org/10.1016/J.ACTAMAT.2017.09.035.
[43] K.A. Christofidou, E.J. Pickering, P. Orsatti, P.M. Mignanelli, T.J.A. Slater, H.J. Stone, N.G. Jones, On the influence of Mn on the phase stability of the $CrMn_xFeCoNi$ high entropy alloys, Intermetallics 92 (2018) 84–92, https://doi.org/10.1016/j.intermet.2017.09.011.
[44] D.G. Shaysultanov, G.A. Salishchev, Y.V. Ivanisenko, S.V. Zherebtsov, M.A. Tikhonovsky, N.D. Stepanov, Novel $Fe_{36}Mn_{21}Cr_{18}Ni_{15}Al_{10}$ high entropy alloy with bcc/B2 dual-phase structure, J. Alloys Compd. (2017), https://doi.org/10.1016/j.jallcom.2017.02.211.
[45] N. Saunders, A.P. Miodownik, CALPHAD (Calculation of Phase Diagrams): a Comprehensive Guide, vol. 1, 1998, https://doi.org/10.1016/S1470-1804(98)80034-5.
[46] O.N. Senkov, J.D. Miller, D.B. Miracle, C. Woodward, Accelerated exploration of multi-principal element alloys for structural applications, Calphad Comput. Coupling Phase Diagrams Thermochem. 50 (2015) 32–48, https://doi.org/10.1016/j.calphad.2015.04.009.
[47] C. Zhang, M.C. Gao, CALPHAD Modeling of High-entropy Alloys, 2016, https://doi.org/10.1007/978-3-319-27013-5_12.
[48] H.L. Chen, H. Mao, Q. Chen, Database development and Calphad calculations for high entropy alloys: challenges, strategies, and tips, Mater. Chem. Phys. (2017), https://doi.org/10.1016/j.matchemphys.2017.07.082.
[49] H. Mao, H.L. Chen, Q. Chen, TCHEA1: a thermodynamic database not limited for “high entropy” alloys, J. Phase Equil. Diffus. 38 (2017) 353–368, https://doi.org/10.1007/s11669-017-0570-7.
[50] W.C. Oliver, G.M. Pharr, Measurement of hardness and elastic modulus by instrumented indentation: advances in understanding and refinements to methodology, J. Mater. Res. 19 (2004) 3–20, https://doi.org/10.1557/jmr.2004.19.1.3.
[51] M.S. Kesler, S. Goyel, O. Rios, D.M. Cupid, H.J. Seifert, F. Ebrahimi, A study of phase transformation in a TiAlNb alloy and the effect of Cr addition, Mater. Sci. Eng. A 527 (2010) 2857–2863, https://doi.org/10.1016/j.msea.2009.12.046.
[52] M.S. Kesler, S. Goyel, F. Ebrahimi, M.V. Manuel, Effect of microstructural parameters on the mechanical behavior of TiAlNb(Cr,Mo) alloys with $\gamma+\sigma$ microstructure at ambient temperature, J. Alloys Compd. 695 (2017) 2672–2681, https://doi.org/10.1016/j.jallcom.2016.11.181.
[53] B. Module, T. Module, P. Models, C.U. Tchea, TCHEA2 : TCS High Entropy Alloy Database 185 Assessed Binary Systems in Full Range of Composition and Temperature, D, 2015. http://www.thermocalc.com/media/35873/tchea2_extended_info.pdf.
[54] Ludmila Tretyachenko and MSIT, Al-Nb-Ti Ternary Phase Diagram Evaluation, 2004. https://materials.springer.com/msi/docs/sm_msi_r_10_016070_02. (Accessed 19 March 2018).
[55] D. Wen, B. Jiang, Q. Wang, F. Yu, X. Li, R. Tang, R. Zhang, G. Chen, C. Dong, Influences of Mo/Zr minor-alloying on the phase precipitation behavior in modified 310S austenitic stainless steels at high temperatures, Mater. Des. 128 (2017) 34–46, https://doi.org/10.1016/j.matdes.2017.04.095.
[56] K. Mahdouk, J.-C. Gachon, L. Bouirden, Enthalpies of formation of the Al–Nb intermetallic compounds, J. Alloys Compd. 268 (1998) 118–121, https://doi.org/10.1016/S0925-8388(97)00554-9.
[57] T. Wang, Z. Jin, J.-C. Zhao, Thermodynamic assessment of the Al-Zr binary system, J. Phase Equil. 22 (2001) 544–551, https://doi.org/10.1361/105497101770332695.
[58] N.D. Stepanov, D.G. Shaysultanov, G.A. Salishchev, M.A. Tikhonovsky, E.E. Oleynik, A.S. Tortika, O.N. Senkov, Effect of v content on microstructure and mechanical properties of the $CoCrFeMnNiV_x$ high entropy alloys, J. Alloys Compd. 628 (2015) 170–185, https://doi.org/10.1016/j.jallcom.2014.12.157.
[59] C.-C. Hsieh, W. Wu, Overview of intermetallic sigma (σ) phase precipitation in stainless steels, ISRN Metall. 2012 (2012) 1–16, https://doi.org/10.5402/2012/732471.